HHS Public Access

Author manuscript

Nature. Author manuscript; available in PMC 2014 May 14.

Published in final edited form as:

Nature. 2013 November 14; 503(7475): 290–294. doi:10.1038/nature12644.

A high-resolution map of three-dimensional chromatin interactome in human cells

Fulai Jin[1,*], **Yan Li**[1,*], **Jesse R. Dixon**[1], **Siddarth Selvaraj**[1], **Zhen Ye**[1], **Ah Young Lee**[1], **Chia-An Yen**[1], **Anthony D. Schmitt**[1], **Celso Espinoza**[1], and **Bing Ren**[1,2,#]

[1]Ludwig Institute for Cancer Research, 9500 Gilman Drive, La Jolla, California 92093, USA

[2]Department of Cellular and Molecular Medicine, Institute of Genome Medicine, Moores Cancer Center, University of California, San Diego, School of Medicine, 9500 Gilman Drive, La Jolla, California 92093, USA

Abstract

A large number of *cis*-regulatory sequences have been annotated in the human genome[1,2], but defining their target genes remains a challenge[3]. One strategy is to identify the long-range looping interactions at these elements with the use of chromosome conformation capture (3C) based techniques[4]. However, previous studies lack either the resolution or coverage to permit a whole-genome, unbiased view of chromatin interactions. Here, we report a comprehensive chromatin interaction map generated in human fibroblasts using a genome-wide 3C analysis method (Hi-C)[5]. We determined over one million long-range chromatin interactions at 5–10kb resolution, and uncovered general principles of chromatin organization at different types of genomic features. We also characterized the dynamics of promoter-enhancer contacts upon TNF-α signaling in these cells. Unexpectedly, we found that TNF-α responsive enhancers are already in contact with their target promoters prior to signaling. Such pre-existing chromatin looping, which also exists in other cell types with different extra-cellular signaling, is a strong predictor of gene induction. Our observations suggest that the three-dimensional chromatin landscape, once established in a particular cell type, is rather stable and could influence the selection or activation of target genes by a ubiquitous transcription activator in a cell-specific manner.

We carried out Hi-C experiments to study the dynamic chromatin interactions in a primary human fibroblast cells (IMR90) in response to transient TNF-α signaling. Combining the Hi-C data from IMR90 cells before and after 1hr TNF-α treatment, we obtained a total of

---

[#]Correspondence and requests for materials should be addressed to B.R. (biren@ucsd.edu).
[*]These authors contributed equally to this work.

Supplementary Information is linked to the online version of the paper at www.nature.com/nature

Author Contributions: YL, FJ and BR designed the studies. YL conducted most of the experiments; FJ carried out the data analysis; JRD, ZY, AYL, CY, ADS and CE contributed to the experiments; SS contributed to the data analysis; FJ, YL and BR prepared the manuscript.

Author Information: All sequencing data described in this study have been deposited to GEO under the accession number GSE43070. Some sequencing data used in this study were previously published and accession numbers can be found in Supplementary Methods. All chromatin interactions called in IMR90 cells can be found in Supplementary Data.

The authors declare no competing financial interests.

~3.4 billion uniquely mapped paired-end reads from 6 biological replicates in each condition, among which ~1.4 billion are intra-chromosomal reads (Supplementary Table S1–S2). In order to accurately identify chromatin looping interactions with high sensitivity and resolution, we devised an improved data filtering strategy[6] based on the strand orientation of Hi-C paired-end reads (Supplementary Fig. 1–6, Supplementary Methods), which results in over 500 million high-confidence read pairs (Supplementary Table S1–S2), each representing a legitimate ligation event between two restriction fragments on the same chromosome. Recognizing that some reads may be due to random collision events between restriction fragments[4,7], we also estimated the expected frequency between any two restriction fragments, and then fitted a negative binomial model to assess the significance of observed contact frequency (Supplementary Methods, Supplementary Fig. 7–9). Compared to previous methods[4], our data analysis method permits detection of chromatin interactions at short distance. For example, we observed asymmetric distribution of *cis*-contacts from highly expressed promoters to the immediate downstream gene bodies (Supplementary Fig. 10). This observation is reminiscent of a recent study showing interactions between a subset of exons and their promoters[8]. Interestingly, while such bias at promoter is correlated with elongation of RNA polymerase II, it remains when transcription elongation is blocked by the pTEF-b inhibitor flavopiridol (Supplementary Fig. 11), suggesting that the maintenance of promoter/gene body contacts is independent of active transcription.

In order to accurately map at high resolution the chromatin interactions genome-wide, we devised an algorithm (Supplementary Fig. 12) to identify statistically significant looping interactions centered on a given genomic region from Hi-C contact matrix (Fig. 1a). Applying this method to the *CCL2* locus, we were able to determine the distal enhancers and CTCF binding sites interacting with the *CCL2* promoter (Fig. 1a–b). Our algorithm also identified a number of previously reported long-range chromatin interactions at the *HoxA* gene cluster[9] and the *SHH* locus[10], which were not readily observable from lower resolution analysis (Supplementary Fig. 13–14). We further performed conventional 3C experiments to validate 6 pairs of long-range interactions identified at 5 different genes, and the results confirmed the reliability of our method (Fig. 1c, Supplementary Fig. 15).

We next applied the above algorithm to the 518,032 anchor regions in the human genome, with each containing one or a few HindIII restriction fragments (fragments shorter than 2kb are merged) (Fig. 2a), and uncovered a total of 1,116,312 chromatin interactions with a false discovery rate (FDR) of 0.1 (Supplementary Data). We found that strong interactions supported by lower p-values and higher contact frequencies are more reproducible between biological replicates (Supplementary Fig. 16). Since interactions between loci separated by more than 2Mb are very rare (Fig. 2c), we limit our search to this genomic span. The sizes of the identified interacting DNA loci range from several hundred base pairs to over 50kb, with a median of 10.5kb (Fig. 2b). We were able to identify chromatin interactions that span a genomic distance from several hundred base pairs to over 1 million base pairs (Fig. 2c). Consistent with previous reports that the genome is partitioned into megabase-sized topological domains[11–13], we found that a majority of the identified chromatin interactions in the IMR90 cells are located within the same topological domains (Fig. 2d, Supplementary Fig. 18).

We next characterized the chromatin interactions centered on the *cis*-elements annotated in the IMR90 cell genome[14] (Supplementary Data). Chromatin looping interactions are significantly enriched at *cis*-regulatory elements, especially active promoters, enhancers and CTCF binding sites, and are rare at inactive TSSs or regions with repressive chromatin domains marked by H3K27me3 (Fig. 2e–f)[15]; notably, both active and poised enhancers (distinguished be the status of H3K27ac)[16–18] are found equally likely to engage looping interactions (Fig. 2e–f), raising the possibility that DNA looping could take place after priming of enhancers by H3K4me1 but before further activation[19]. Interestingly, the chromatin interactions centered on CTCF binding sites tend to occur over a longer range than other types of *cis*-elements (Fig. 2g), confirming a recent result obtained from selected loci[20]. We also explored the spatial organization of *cis*-elements by examining preferential interaction between different classes of elements. Strongest enrichment was observed between H3K27me3 marked regions (Fig. 2h), consistent with the known compact 3D structure at this type of repressive chromatin domains[21] (e.g. Supplementary Fig.14a). The inactive promoters tend to interact with regions depleted of enhancers but enriched for repressive mark H3K27me3 (Fig. 2h), while CTCF binding sites loop to both active and inactive promoters with no preference, as also reported previously[15]. It is also interesting to observe that CTCF binding sites seem to prefer promoters over enhancers (Fig. 2h), suggesting a specific role for CTCF in organizing long-range chromatin interactions to promoters.

Looping interactions between *cis*-regulatory elements and gene promoters have been shown to be important for transcription regulation at a number of loci[3]. The genome-wide identification of chromatin interactions in the IMR90 cells allowed us to examine this concept systematically. We first focused on the looping interactions anchored to gene promoters, and denote the identified interacting sequences as “promoter tethered regions” (PTRs) (Fig. 3a). In IMR90 cells, we found 57,585 PTRs identifying 29,132 enhancer-promoter (EP) pairs involving 6,133 active promoters and 15,432 distal active enhancers (Supplementary Data). Only around 25% of EP pairs are within 50kb range, and ~57% span 100kb or larger genomic distance, with a median distance of 124kb (Fig. 3b). We assigned 55% of distal enhancers to at least one active promoter, and 25% of enhancers to 2 or more active promoters (Fig. 3c, left panel). This result confirms previous observation that promoters and enhancers often form complex networks to regulate transcription[15]. We further hypothesized that genes sharing common enhancers (denoted hub enhancers) are likely to have coordinated gene expression patterns. Indeed, genes sharing the same NF-κB responsive enhancers are more frequently induced together by TNF-α than expected by chance (Fig. 3d). As an example, *CKAP2L* and *IL1A* are induced simultaneously by TNF-α although lacking promoter bound p65 peaks, and they share overlapping distal PTR regions containing multiple NF-κB binding sites (Fig. 3e). Similar examples can be found in other gene clusters co-induced by TNF-α treatment (Supplementary Fig. 19). These results therefore provide a molecular mechanism for coordinated gene expression of neighboring genes.

Interestingly, 46% of the active genes do not interact with any distal enhancer (Fig. 3c, right panel). Gene ontology analysis showed that these genes are enriched with housekeeping

genes (Supplementary Fig. 20a). On the other hand, 54% of the active promoters demonstrate extensive looping interacting with enhancers (average 4.75 enhancers per gene, Fig. 3c, right panel), and they are enriched with genes related to biological pathways such as signal transduction (Supplementary Fig. 20b). This analysis suggests that housekeeping genes, despite being highly transcribed, do not engage a lot of distal regulatory elements. On the other hand, genes involved in cell specific functions are under extensive control of distal regulator sequences.

We next examined long range looping interactions at transcriptional enhancers, focusing on those bound by the p65 subunit of NF-κB transcription factor. Using ChIP-seq, we identified 15,621 p65 binding sites in the genome after TNF-α treatment, 2,315 (14.8%) of which can be classified as "active p65 binding sites" because they exhibit increased H3K27ac levels and eRNA expression upon TNF-α signaling (Supplementary Fig. 21–22). Consistent with their putative role in mediating transcriptional induction, these "active p65 binding sites" are enriched near TNF-α dependent genes (Supplementary Fig. 22c). We next tested if the long-range interactions between these p65 binding sites and their target promoters are correlated with transcriptional induction. Indeed, at the promoters that exhibit interactions with one or more active p65 binding sites, significantly higher levels of transcriptional induction were observed than the promoters that do not interact with distal p65 binding sites (Fig. 3f), suggesting that the identified long-range chromatin interactions may play a key role in transcriptional regulation of the TNF-α inducible genes.

The high-resolution map of chromatin interactions may also improve the prediction of target genes of distal enhancers. Currently, a common practice is to assign distal enhancers to their nearest promoters, assuming one enhancer is linked to just one target gene (proximity approach). This approach, however, cannot explain all of the 828 TNF-α responsive genes. We found 331 (40%) of these genes have one or more p65 binding sites within 2.5kb of their promoters, and 362 genes of the remainder can be assigned to one or more NF-κB binding sites by proximity approach, leaving still 135 TNF-α induced gene unexplained. Using a recently published enhancer-promoter connection map[22] based on correlated chromatin features across diverse tissues or cell types, we were able to link 10 of the 135 unexplained TNF-α inducible genes to distal NF-κB binding sites. Using the chromatin interactome map, 74 (55%) of the unexplained genes can be assigned to a NF-κB binding site (Supplementary Fig. 23). This result illustrates that the chromatin interactome map described here could be valuable for the study of long-range regulation of gene expression by transcription factors.

We found no obvious alterations of mega-base topological domains[12] in IMR90 cells upon TNF-α treatment (for example, Supplementary Fig. 13). Since previous studies have shown that gene activation by enhancers is accompanied by alteration of chromatin interactions[3,23,24], we expected that at shorter distance, binding of NF-κB to enhancers would induce looping interactions that bring the distal enhancers to proximity with target genes. To our surprise, we found that at the vast majority of TNF-α responsive enhancers, there is little change of DNA looping after treatment (Fig. 4a). These results suggest that in general, enhancer-promoter interactions already form in untreated cells; and these pre-existing DNA-structures are not significantly altered by transient activation or repression of enhancers. 3C assays confirm that DNA looping exists at several loci prior to TNF-α

treatment (Fig. 1e, Supplementary Fig. 15a–c). We further compared the normalized reads count anchored to the TNF-α activated enhancers at different ranges of genomic distances (Fig. 4b, Supplementary Methods). Consistent with the results in Fig. 4a, transient activation of p65 bound enhancers does not lead to significant changes in chromatin interactions (Fig. 4b). By contrast, the chromatin interactions (especially within a short genomic distance) at cell type specific enhancers are highly variable between cell types (Fig. 4c–d), suggesting the existence of specific chromatin interaction structures at cell type specific enhancers. Interestingly, the discrepancy between signal-dependent and cell-type specific enhancers is well correlated with the levels of H3K4me1 at those dynamically regulated enhancers: Despite the quick induction of H3K27ac mark at TNF-α responsive enhancers, strength of H3K4me1 signal are largely unchanged (Fig. 4e); on the other hand, cell type specific enhancers have highly cell-specific H3K4me1 occupancy (Fig. 4f).

Recently, pre-existing promoter-enhancer looping was reported at several loci induced by p53, FOXO3 and glucocorticoid receptor using 4C approach[20,25,26]. Our genome-wide analysis of chromatin interactome maps in IMR90 cells suggests that this is likely a common rule rather than a special case. To further demonstrate its generality, we examined 6 additional promoter-enhancer pairs by 3C assays in four different cell types (IMR90, HUVEC, MCF7 and LNCaP cells) under different stimuli (IFN-γ, TNF-α, β-estradiol and 5α-dihydrotestosterone, respectively). In all of these examples, we found evident pre-existing promoter-enhancer contacts, and the looping interactions are largely unchanged after enhancer activation and target gene induction (Supplementary Fig 15d, 24). Our results predict that pre-existing chromatin looping interactions could dictate the spectrum of the target genes for a transcription factor even before it is activated. Indeed, p65 binding sites looping to the promoters prior to induction are much more likely to result in transcriptional activation of the linked gene than otherwise (Fig. 4g). This trend is especially obvious when the p65-binding sites are located far from the linked promoters. Based on this observation, we conclude that pre-existing DNA-looping interactions between enhancers and promoters allow a ubiquitous, signal-dependent transcription factor to affect a selected set of genes in a cell type specific manner.

In summary, we demonstrated that enhancer/promoter interactions already form in each cell type prior to the binding of signal dependent transcription factors, and they undergo little change during transient transcriptional activation. Several recent genome-wide studies have revealed that in different cell type, the repertoire of specific enhancers provides a unique context for the activation of different transcriptional programs in response to signal dependent transcription factors including NF-κB[19,27–30]. Here, our results further suggest that targets of cell-specific enhancers are already hardwired into the chromatin architecture. We therefore propose that cell type-specific looping structure, by controlling the accessibility of the enhancers to their specific targets, may form an additional layer of regulation in determining the distinct transcription programs in different cell types.

Methods summary

Hi-C experiments were performed in human primary IMR90 fibroblasts. ChIP-Seq, GRO-Seq, or RNA-seq libraries were also generated from IMR90, HUVEC, MCF7 or LNCaP

cells and sequenced on the Illumina Hi-Seq2000 platform. All the reads were mapped to reference human genome (hg18). More information about the experiments and detailed descriptions of Hi-C data analysis pipeline, including data filtering, normalization, statistical modeling and interaction calling can be found in Supplementary Methods.

Supplementary Material

Refer to Web version on PubMed Central for supplementary material.

Acknowledgements

We thank Christopher K Glass for sharing the GRO-Seq protocol, Samantha Kuan and Lee Edsall for assistance with high-throughput DNA sequencing and the initial processing. This work is supported by funds from the Ludwig Institute for Cancer Research, the California Institute of Regenerative Medicine (RN2-00905) and US National Institutes of Health (P50 GM085764-03).

Reference

1. Bernstein BE, et al. An integrated encyclopedia of DNA elements in the human genome. Nature. 2012; 489:57–74. [PubMed: 22955616]
2. Maurano MT, et al. Systematic localization of common disease-associated variation in regulatory DNA. Science (New York, N.Y. 2012; 337:1190–1195.
3. Smallwood A, Ren B. Genome organization and long-range regulation of gene expression by enhancers. Current opinion in cell biology. 2013; 25:387–394. [PubMed: 23465541]
4. Dekker J, Marti-Renom MA, Mirny LA. Exploring the three-dimensional organization of genomes: interpreting chromatin interaction data. Nature reviews. 2013; 14:390–403.
5. Lieberman-Aiden E, et al. Comprehensive mapping of long-range interactions reveals folding principles of the human genome. Science (New York, N.Y. 2009; 326:289–293.
6. Imakaev M, et al. Iterative correction of Hi-C data reveals hallmarks of chromosome organization. Nature methods. 2012; 9:999–1003. [PubMed: 22941365]
7. de Wit E, de Laat W. A decade of 3C technologies: insights into nuclear organization. Genes & development. 2012; 26:11–24. [PubMed: 22215806]
8. Mercer TR, et al. DNase I-hypersensitive exons colocalize with promoters and distal regulatory elements. Nature genetics. 2013
9. Noordermeer D, et al. The dynamic architecture of Hox gene clusters. Science (New York, N.Y. 2011; 334:222–225.
10. Lettice LA, et al. Disruption of a long-range cis-acting regulator for Shh causes preaxial polydactyly. Proceedings of the National Academy of Sciences of the United States of America. 2002; 99:7548–7553. [PubMed: 12032320]
11. Zhang Y, et al. Spatial organization of the mouse genome and its role in recurrent chromosomal translocations. Cell. 2012; 148:908–921. [PubMed: 22341456]
12. Dixon JR, et al. Topological domains in mammalian genomes identified by analysis of chromatin interactions. Nature. 2012; 485:376–380. [PubMed: 22495300]
13. Sexton T, et al. Three-dimensional folding and functional organization principles of the Drosophila genome. Cell. 2012; 148:458–472. [PubMed: 22265598]
14. Hawkins RD, et al. Distinct epigenomic landscapes of pluripotent and lineage-committed human cells. Cell stem cell. 2010; 6:479–491. [PubMed: 20452322]
15. Sanyal A, Lajoie BR, Jain G, Dekker J. The long-range interaction landscape of gene promoters. Nature. 2012; 489:109–113. [PubMed: 22955621]
16. Creyghton MP, et al. Histone H3K27ac separates active from poised enhancers and predicts developmental state. Proceedings of the National Academy of Sciences of the United States of America. 2010; 107:21931–21936. [PubMed: 21106759]

17. Hawkins RD, et al. Dynamic chromatin states in human ES cells reveal potential regulatory sequences and genes involved in pluripotency. Cell research. 2011; 21:1393–1409. [PubMed: 21876557]
18. Rada-Iglesias A, et al. A unique chromatin signature uncovers early developmental enhancers in humans. Nature. 2010; 470:279–283. [PubMed: 21160473]
19. Heinz S, et al. Simple combinations of lineage-determining transcription factors prime cis-regulatory elements required for macrophage and B cell identities. Molecular cell. 2010; 38:576–589. [PubMed: 20513432]
20. Phillips-Cremins JE, et al. Architectural Protein Subclasses Shape 3D Organization of Genomes during Lineage Commitment. Cell. 2013; 153:1281–1295. [PubMed: 23706625]
21. Francis NJ, Kingston RE, Woodcock CL. Chromatin compaction by a polycomb group protein complex. Science (New York, N.Y. 2004; 306:1574–1577.
22. Thurman RE, et al. The accessible chromatin landscape of the human genome. Nature. 2012; 489:75–82. [PubMed: 22955617]
23. Ong CT, Corces VG. Enhancer function: new insights into the regulation of tissue-specific gene expression. Nature reviews. 2011; 12:283–293.
24. Schoenfelder S, Clay I, Fraser P. The transcriptional interactome: gene expression in 3D. Current opinion in genetics & development. 2010; 20:127–133. [PubMed: 20211559]
25. Melo CA, et al. eRNAs are required for p53-dependent enhancer activity and gene transcription. Molecular cell. 2013; 49:524–535. [PubMed: 23273978]
26. Tan PY, et al. Integration of regulatory networks by NKX3-1 promotes androgen-dependent prostate cancer survival. Molecular and cellular biology. 2012; 32:399–414. [PubMed: 22083957]
27. Jin F, Li Y, Ren B, Natarajan R. PU.1 and C/EBP(alpha) synergistically program distinct response to NF-kappaB activation through establishing monocyte specific enhancers. Proceedings of the National Academy of Sciences of the United States of America. 2011; 108:5290–5295. [PubMed: 21402921]
28. John S, et al. Chromatin accessibility pre-determines glucocorticoid receptor binding patterns. Nature genetics. 2011; 43:264–268. [PubMed: 21258342]
29. Mullen AC, et al. Master transcription factors determine cell-type-specific responses to TGF-beta signaling. Cell. 2011; 147:565–576. [PubMed: 22036565]
30. Jin F, Li Y, Ren B, Natarajan R. Enhancers: multi-dimensional signal integrators. Transcription. 2011; 2:226–230. [PubMed: 22231119]

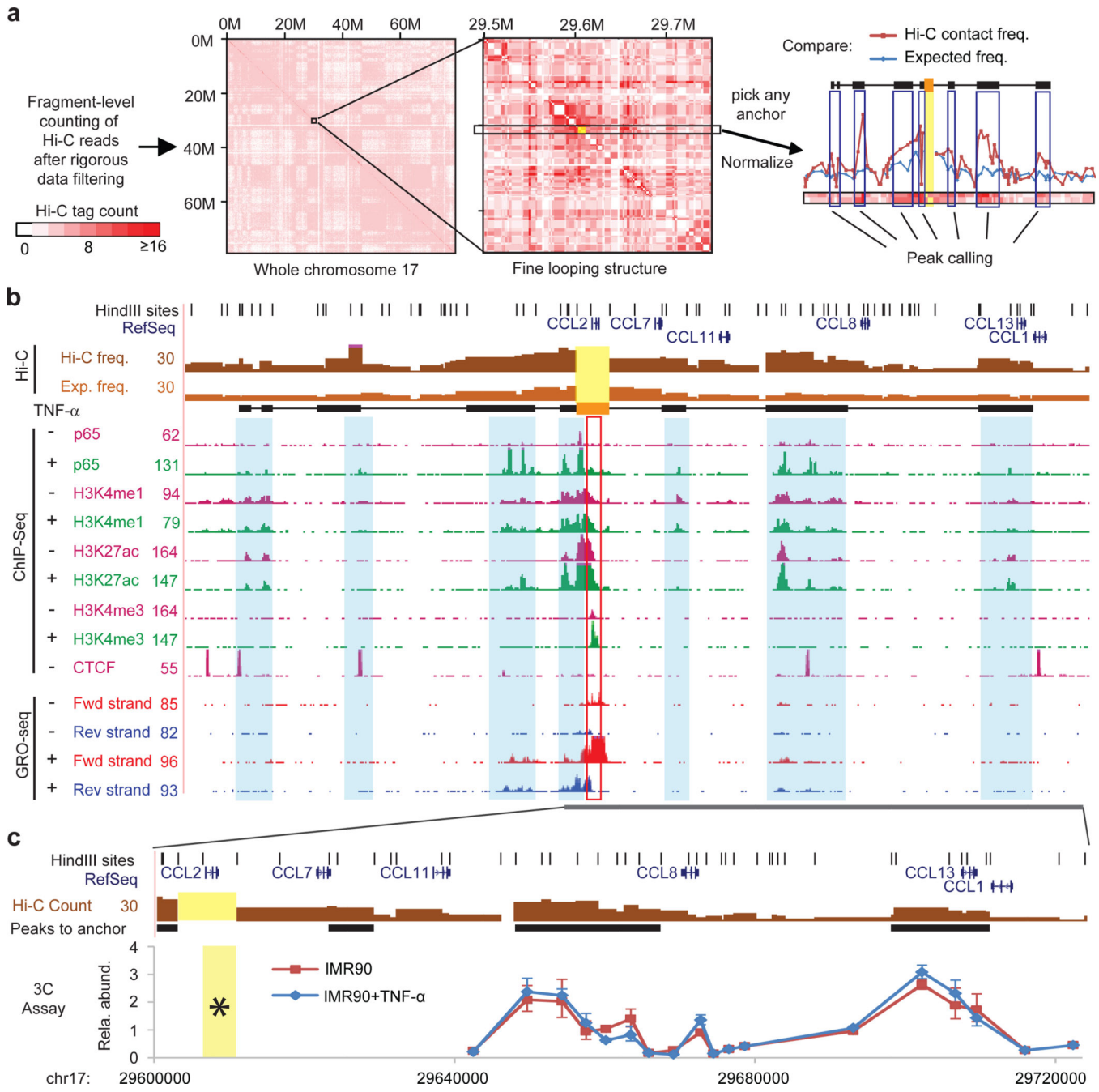

Figure 1. Fine mapping of chromatin interactions in IMR90 cells

a, An illustration of the Hi-C data analysis procedure to identify regions interacting with a selected genomic region, such as the *CCL2* locus as highlighted in yellow (Supplementary Method). **b**, Genome browser shot of the *CCL2* locus showing the results from Hi-C, ChIP-seq and Gro-seq experiments. Each bar in the top 2 tracks are either Hi-C reads count (dark brown) or expected frequency (light brown) from a fragment to *CCL2* locus (highlighted in yellow and orange filled box). Black filled boxes are regions interacting with *CCL2* called by the peak calling algorithm same as the black filled boxes in (**a**). Light blue shadows highlight the enhancer/CTCF locations from ChIP-seq data. *CCL2* is induced by TNF-α

(shown in the GRO-Seq tracks). **c**, Validation of the DNA looping interactions with *CCL2* using 3C assays. Yellow: anchor fragments in Hi-C or 3C (with star). Error bar: *s.d.* from 3 PCR replicates.

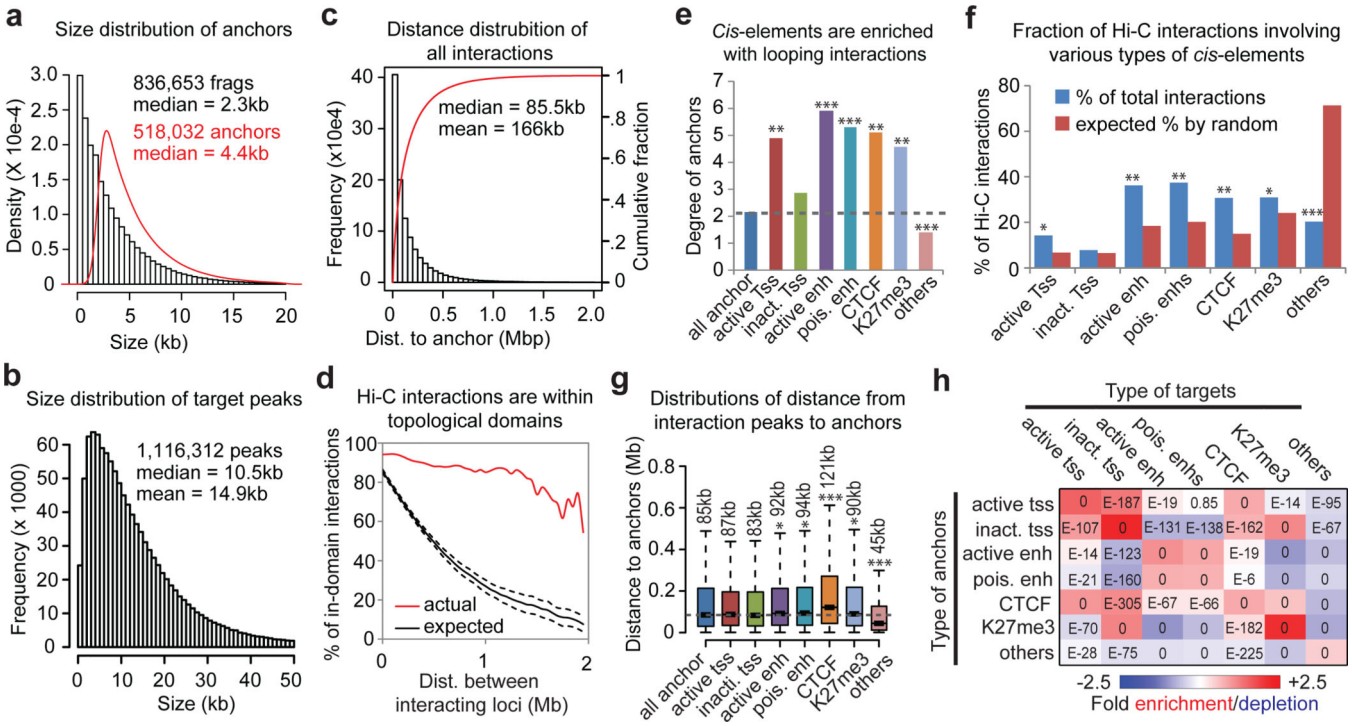

Figure 2. Characterization of the IMR90 chromatin interactome

a, Histogram showing the size distribution of all HindIII restriction fragments in human genome. The red curve plots the size distribution of all anchors used in this study. **b**, Size distribution of the genomic regions identified as interacting with all anchors. **c**, Distribution of genomic spans of all identified chromatin interactions. Histogram: frequency distribution; Red curve: cumulative fraction with increasing distances. **d**, Fraction of chromatin looping interactions that fall within the same topological domains is plotted as a function of genomic distance between the two interacting loci (red curve). Black curve: expected fraction calculated from random shuffling locations of topological domains (100 iterations, dashed error lines: *s.d.*). **e**, Average number of peaks identified for anchors with different *cis*-elements. **f**, Percentages of all interactions involving various types of *cis*-elements (either anchor or target peak has the elements). In **e–f**, *Z*-scores were calculated comparing the actual values to simulation by randomly shuffling the locations of *cis*-elements (100 iterations, two-side *Z*-test). * $Z > 50$, ** $Z > 100$, *** $Z > 150$. **g**, Box plot showing the distance distribution from different types of anchors to their targets. Median distances are also labeled. *t*-statistics are computed comparing log-transformed distance between each type of anchors to all anchors as control (dash horizontal line). * $t > 20$, ** $t > 40$, *** $t > 80$ (two-side *t*-test). **h**, Preferential interactions between different types of *cis*-elements. Heatmap shows the fold enrichment of different type of pair-wise combinations. *p*-values are computed using hypergeometric test and denoted in each cell.

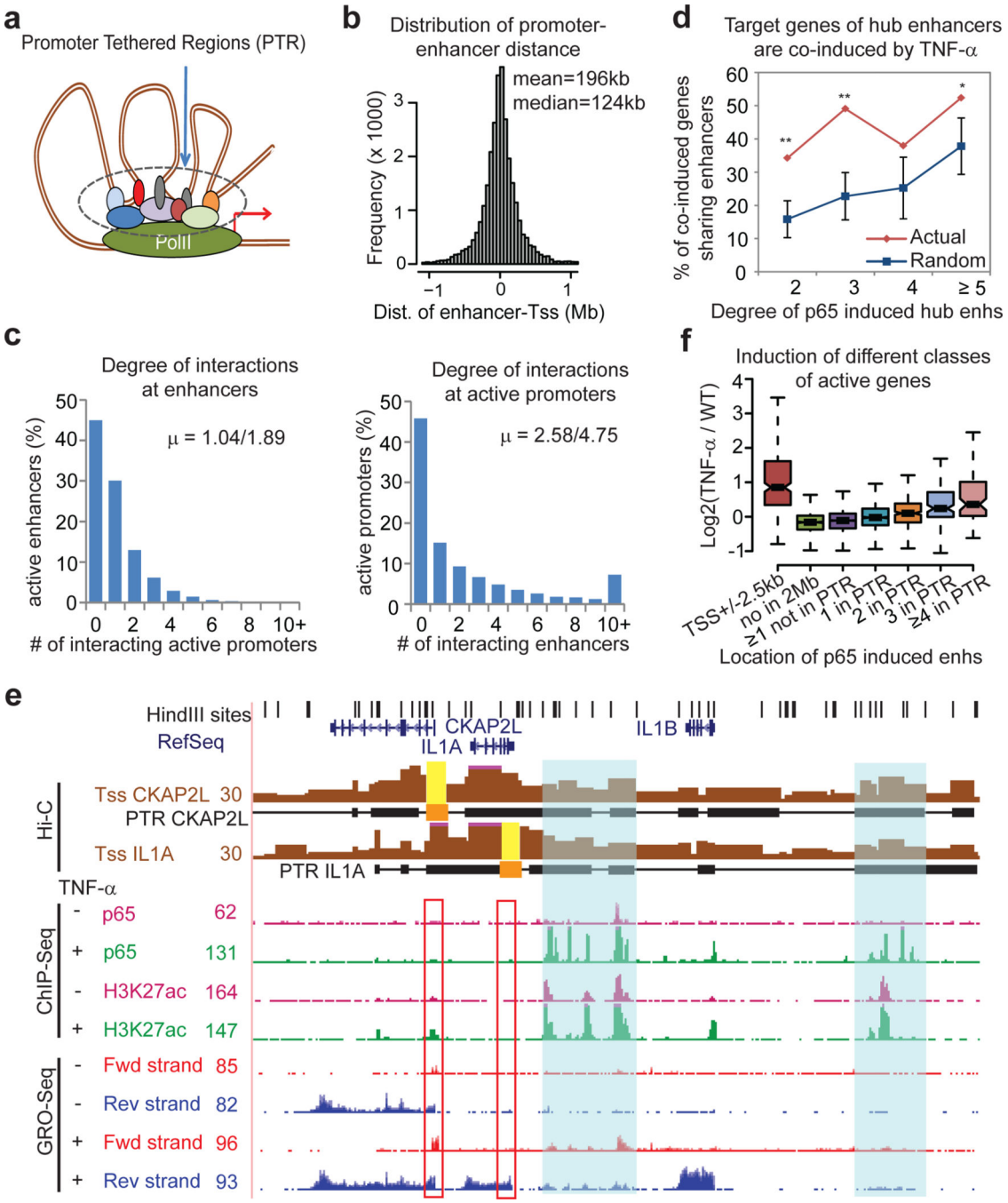

Figure 3. Identification and characterization of promoter-enhancer interactions in IMR90 cells

a, A schematic of promoter tethered regions (PTRs). **b**, Distribution of distances between the promoters and enhancers found within the PTRs. **c**, Bar charts show the degrees of interactions. Left: Percentage of enhancers that are looped to active promoters found in PTRs. The first value of μ is the mean degree of promoter interactions for all enhancers; the second value is the mean degree of promoter interactions for enhancers interacting with at least one promoter. Right: distribution of degrees of enhancer interactions for active promoters. **d**. Genes sharing enhancers are co-regulated. Among the target genes of TNF-α

responsive hub enhancers, proportion of co-induced gene pairs (> 2-fold) are plotted and compared to random simulation (100 iterations, two-side *Z*-test, * $p < 0.05$, ** $p < 0.01$, error bar: *s.d.*) **e**, Genome browser snapshots showing the virtual 3C plots of the *CKAP2L* and *IL1A* promoters. **f**, Compare the induction of different gene groups based on the location of p65 induced enhancers.

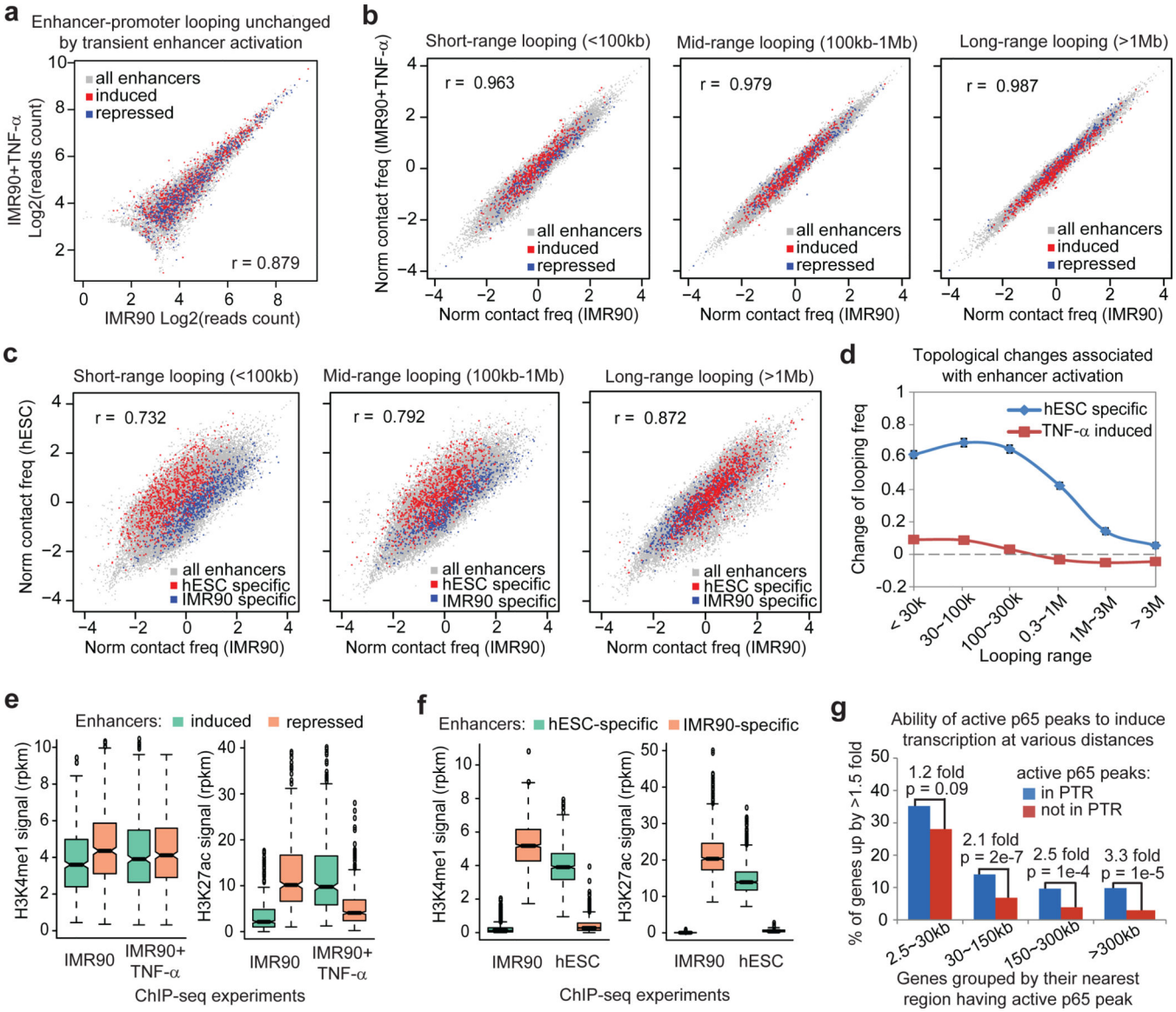

Figure 4. The higher order chromatin structure in IMR90 cells is stable during transient TNF-α signaling

a, A scatter plot comparing reads count at PTRs before and after TNF-α treatment. Grey dots are data for PTRs involving all enhancers, red or blue dots are PTRs involving the top 500 induced or repressed enhancers, respectively. *r*: Pearson's Correlation calculated from all data points. **b**, Scatter plots compare normalized contact frequencies (Supplementary Methods) of all enhancers before and after 1 hr TNF-α stimulation. **c**, Scatter plots compare contact frequencies of enhancers in IMR90 and hESC cells. Colored points represent the top 2,000 hESC- (red) or IMR90-specific (blue) enhancers defined by H3K27ac mark. **d**, The relative change of contact frequency (comparing to untreated IMR90 cells) at hESC-specific or TNF-α induced enhancers are plotted in line graphs. **e**, Box plots of H3K4me1 and H3K27ac signals on enhancers that show increased or decreased H3K27ac signals after TNF-α treatment. **f**, Boxplots of H3K4me1 and H3K27ac ChIP-seq signals at the IMR90 or

hESC specific enhancers. **g**, Bar charts showing that NF-κB binding sites within PTRs are more likely to activate target genes than those outside PTRs. In this figure, PTRs are identified using the Hi-C data from untreated IMR90 cells. The *p*-values are calculated using hypergeometric test.